Experimental implementation of a nonlinear beamsplitter based on a phase-sensitive parametric amplifier

Yami Fang, Jingliang Feng, Leiming Cao, Yaxian Wang, and Jietai Jing

Citation: Appl. Phys. Lett. **108**, 131106 (2016); doi: 10.1063/1.4945260
View online: http://dx.doi.org/10.1063/1.4945260
View Table of Contents: http://aip.scitation.org/toc/apl/108/13
Published by the American Institute of Physics

Experimental implementation of a nonlinear beamsplitter based on a phase-sensitive parametric amplifier

Yami Fang, Jingliang Feng, Leiming Cao, Yaxian Wang, and Jietai Jing[a)]
State Key Laboratory of Precision Spectroscopy, East China Normal University, Shanghai 200062, China

(Received 13 October 2015; accepted 21 March 2016; published online 29 March 2016)

Beamsplitters have played an important role in quantum optics experiments. They are often used to split and combine two beams, especially in the construct of an interferometer. In this letter, we experimentally implement a nonlinear beamsplitter using a phase-sensitive parametric amplifier, which is based on four-wave mixing in hot rubidium vapor. Here we show that, despite the different frequencies of the two input beams, the output ports of the nonlinear beamsplitter exhibit interference phenomena. We make measurements of the interference fringe visibility and study how various parameters, such as the intensity gain of the amplifier, the intensity ratio of the two input beams, and the one and two photon detunings, affect the behavior of the nonlinear beamsplitter. It may find potential applications in quantum metrology and quantum information processing. © *2016 AIP Publishing LLC*. [http://dx.doi.org/10.1063/1.4945260]

A beamsplitter is an elementary optical device that splits a beam of light into two, which has played an irreplaceable role in quantum optics.[1] It has been theoretically studied and experimentally used to generate multipartite entanglement[2,3] and Gaussian cluster states.[4–9] More importantly, it is the crucial part of most interferometers. For example, the Mach-Zehnder interferometer consists of two beamsplitters, with one acting as a wave splitter and the other as a wave combiner. The fully quantum description of a beamsplitter can be found in Ref. 1.

More recently, our group has experimentally built a nonlinear interferometer with two parametric amplifiers (PAs),[10–12] which can reach the ultimate quantum limit of phase measurement, i.e., the Heisenberg limit.[13,14] Specifically, the parametric amplifier is based on nondegenerate four-wave mixing (FWM) process in two hot Rb-85 atomic vapor cells.[15–18] It has several advantages for practical implementations, for example, no need of cavity due to strong nonlinearity of the system and thus no mode constraints, spatial separation of the generated nonclassical beams and thus making the system simple, etc. It has been proved to be a very promising candidate in quantum information processing and has many applications such as quantum entangled imaging,[19] tunable delay of EPR entangled states,[20] low-noise amplification of an entangled state,[21] realization of slow, fast or stopped light,[22–24] high purity narrow-bandwidth single photons generation,[25] advancement of quantum correlation,[26,27] generation of three strongly quantum correlated beams,[28] ultrasensitive measurement of microcantilever displacement[29] and the localized multi-spatial-mode quadrature squeezing for quantum imaging.[30]

In our nonlinear interferometer, the first PA amplifies the "signal" (probe) beam and generates a new "idler" (conjugate) beam. After that, both beams are sent to the second identical PA. Thus, the first one acts as a wave splitter and the second one as a wave combiner. Since amplification is involved in both PAs, we can consider them as nonlinear beamsplitters. Recently, we have theoretically proposed versatile quantum networks for generation of cluster state by cascading several phase-insensitive PAs[31] or utilizing the optical spatial mode comb,[32] making the so-called nonlinear quantum networks.

Unlike the PAs mentioned above, which are seeded by either one coherent beam or two quantum-correlated beams,[10–12,31,32] here we experimentally realized another type of nonlinear beamsplitter, which combines two incoming optical fields in coherent state with different frequencies. This is actually the proposal for two-mode phase sensitive amplifier (PSA) that we have theoretically studied recently.[33] We will also show that the output ports of this type of nonlinear beamsplitter exhibit interference phenomena and study how the various experimental parameters such as the intensity gain of the amplifier, the intensity ratio of the two input beams, one-photon detuning and two-photon detuning, affect the behavior of interference.

As shown in Fig. 1(a), a normal beamsplitter combines two input beams with same frequency and induces interference phenomena at the two output ports. Considering the schematic shown in Fig. 1(b), two beams with different frequencies are injected to a nonlinear beamsplitter, which is based on parametric amplification process. The input-output relation of a PA is well described by

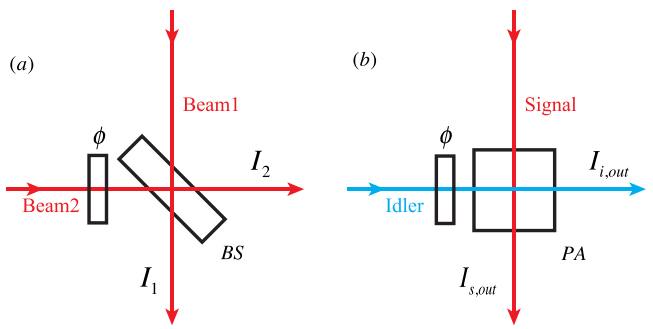

FIG. 1. BS, beamsplitter; PA, parametric amplifier; ϕ, the phase shift of beam2 or idler beam; $I_1, I_2, I_{s,out}, I_{i,out}$, the intensities of the output beams. (a) A normal beamsplitter combining two beams. (b) A nonlinear beamsplitter based on a PA.

a)Electronic mail: jtjing@phy.ecnu.edu.cn

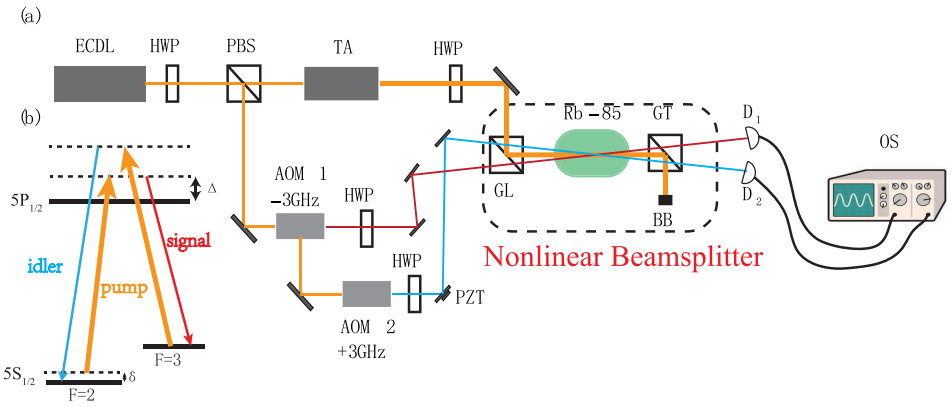

FIG. 2. Experimental layout. (a) ECDL, external cavity diode laser; HWP, half wave plate; PBS, polarization beamsplitter; TA, tapered amplifier; AOM, acousto-optic modulator; PZT, piezo-electric transducer; GL, Glan-Laser polarizer; GT, Glan-Thompson polarizer; BB, beam blocker; D1, D2, photodetectors; OS, oscilloscope. (b) Double-Λ scheme of the D1 line of Rb-85. Δ, one-photon detuning; δ, two-photon detuning.

$$\hat{a}_{out} = \sqrt{G}\hat{a}_{in} + e^{i\phi}\sqrt{G-1}\hat{b}^{\dagger}_{in}, \tag{1}$$

$$\hat{b}^{\dagger}_{out} = e^{-i\phi}\sqrt{G-1}\hat{a}_{in} + \sqrt{G}\hat{b}^{\dagger}_{in}, \tag{2}$$

where G is the intensity gain and a (b) indicates the signal (idler) field. Here, we assume that the idler beam is subject to a phase shift of ϕ, while the phases of the signal and pump beams are fixed.

When both input ports are seeded by coherent fields, the intensities of the output fields are given by

$$I_{s,out} = GI_a + (G-1)I_b + 2\sqrt{G(G-1)I_aI_b}\cos\phi, \tag{3}$$

$$I_{i,out} = GI_b + (G-1)I_a + 2\sqrt{G(G-1)I_aI_b}\cos\phi, \tag{4}$$

where I_a and I_b indicate the intensities of the input fields. Here, we have neglected the spontaneous emission term G-1,[33] since both input beams (in μW order, corresponding to photon number of 4×10^{12} within 1 s) are bright in experiment. From Eqs. (3) and (4), one can easily find that the output fields can be amplified or de-amplified under varying phase, leading to the interference phenomena at the two output ports. The interference visibilities for both output ports are calculated

$$V_s = \frac{2\sqrt{\beta}\sqrt{G(G-1)}}{\beta G + G - 1}, \tag{5}$$

$$V_i = \frac{2\sqrt{\beta}\sqrt{G(G-1)}}{\beta G + G - \beta}, \tag{6}$$

where $\beta = I_a/I_b$. The interference phenomena can be explained as two individual PAs seeded only by the signal or idler field interfering with each other. Each PA amplifies or generates its own signal and idler beams, respectively. The two output signal beams of the same frequency are well overlapped under our current symmetric geometry and so are the two output idler beams. Thus, these two output signal (idler) beams will interfere with each other, leading to the amplification or de-amplification of the beams. From this point of view, our nonlinear beamsplitter induces interference phenomena at each output port.

The experimental layout is shown in Fig. 2. The nonlinear beamsplitter is based on a double-Λ configuration FWM process in a Rb-85 vapor cell (as shown in Fig. 2(b)). We use an external cavity diode laser (ECDL) and a tapered amplifier (TA) as our laser system. The linewidth of the ECDL is of 100 kHz and the frequency is blue detuned about 0.8 GHz to the $5S_{1/2}, F = 2 \rightarrow 5P_{1/2}$ transition. A polarization beamsplitter (PBS) is used to split the beam into two. One is sent to the TA to generate the pump beam which is vertically polarized. The other one is passed through an acousto-optic modulator (AOM1). A weak signal beam tuned 3.04 GHz to the red side of the pump is derived. Afterwards, the zero order beam passed through the first AOM is sent to the second AOM. In the same way, a weak idler beam tuned 3.04 GHz to the blue side of the pump is produced. Both signal and idler beams are horizontally polarized. All these beams are combined with a Glan-Laser polarizer and crossed at the center of the Rb vapor cell, whose temperature is stabilized at 116 °C. The beam waist of the signal (idler) beam is 200 (215) μm, and 500 μm for the pump beam. A Glan-Thompson polarizer with an extinction ratio of $10^5 : 1$ is placed after the cell to filter out the residual pump beam. The output signal and idler beams are sent to two photodetectors (D_1 and D_2).

As shown in Fig. 3, the typical interference fringes of the two outputs are obtained by scanning the piezo-electric transducer mirror on the input idler beam path. The interference visibilities of the signal and idler output ports are 91.6% and 90.0% respectively. It should be pointed out that the data of visibility of the signal and idler beams are not measured at the same time. The two interference fringes are modulated in sync in principle. The output fields can be amplified (above the straight green lines) or de-amplified (below the straight

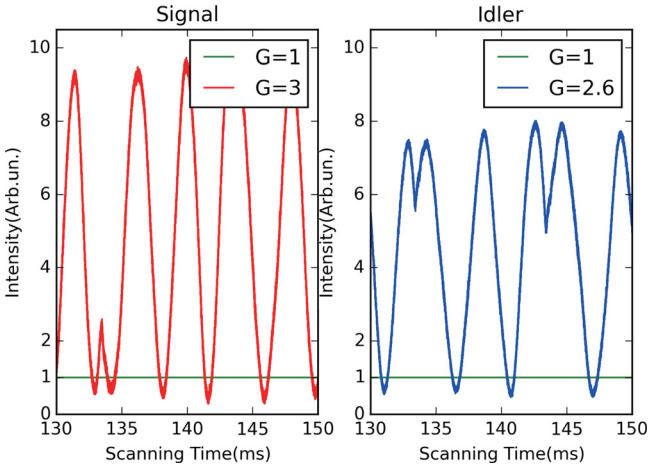

FIG. 3. Interference fringes at the output ports of the nonlinear beamsplitter. Left, Signal output. Right, Idler output. The green lines, the output of signal/idler without the pump beam.

green lines) by this nonlinear beamsplitter depending on the value of phase ϕ. The measured intensities of the two output beams when the pump beam is blocked are defined as unit and denoted by the straight green lines in Fig. 3. The interference pattern intensities of both output beams are normalized to the two straight green lines, respectively.

In order to investigate the influence of intensity ratio β between the two input beams on the visibilities of the two output ports, we keep the idler beam power (10 μW) unchanged and vary the signal beam power from 2.5 μW to 40 μW. At the same time, we change the intensity gain of the system by varying the pump beam power. The other parameters are set as follows: $\delta = 4$ MHz and $\Delta = 0.8$ GHz. The experimental results (Bottom) and theoretical predictions (Top) agree very well, as shown in Fig. 4. For the experimental results, the maximal visibilities for both the signal and idler beams are limited by absorption losses and imperfect spatial mode matching between the input beams at the center of the vapor cell. At large intensity gain regime, the better intensity balancing of the two input beams gives better visibilities.

The one-photon detuning and two-photon detuning of the system can affect the behavior of the nonlinear beamsplitter. Therefore, the visibilities also will be influenced by these two parameters. To study this effect, we fix the signal and idler beam powers at 20 μW. First, we set the two-photon detuning at 4 MHz and scan the one-photon detuning from 0.4 GHz to 2.0 GHz. At the same time, we record the intensity gains and visibilities of two output ports. The results are shown in Fig. 5(a). The red diamond trace is for the signal visibility as a function of one-photon detuning and the blue diamond trace is for the idler. The green and yellow dot traces are for the intensity gains of the signal and idler beams, respectively. Within the range from 0.5 GHz to 1.0 GHz, the visibilities for both channels are all above 90%. Both of the intensity gains decrease as the detuning increases. Second, we set the one-photon detuning at 0.8 GHz and scan the two-photon detuning from −5 MHz to 65 MHz. We vary the frequencies of both signal and idler beams symmetrically to change the two-photon detuning. The results are shown in Fig. 5(b). We find that the visibilities keep above 90% within a wide range from 0 MHz to 30 MHz. The best visibility for both output ports is achieved at about 4 MHz.

It must be pointed out that our nonlinear beamsplitter described in this letter is different from both stages of our previous SU (1,1) interferometer.[10–12] In our previous SU (1,1) interferometer, the first PA works in phase-insensitive configuration, and it amplifies the signal beam and generates a idler beam. The signal and idler beams are quantum-correlated and very noisy after this amplification (well above their corresponding shot noise limits). The second PA is injected with signal, idler, and pump beams and thus becomes phase-sensitive. The gain of the second PA will

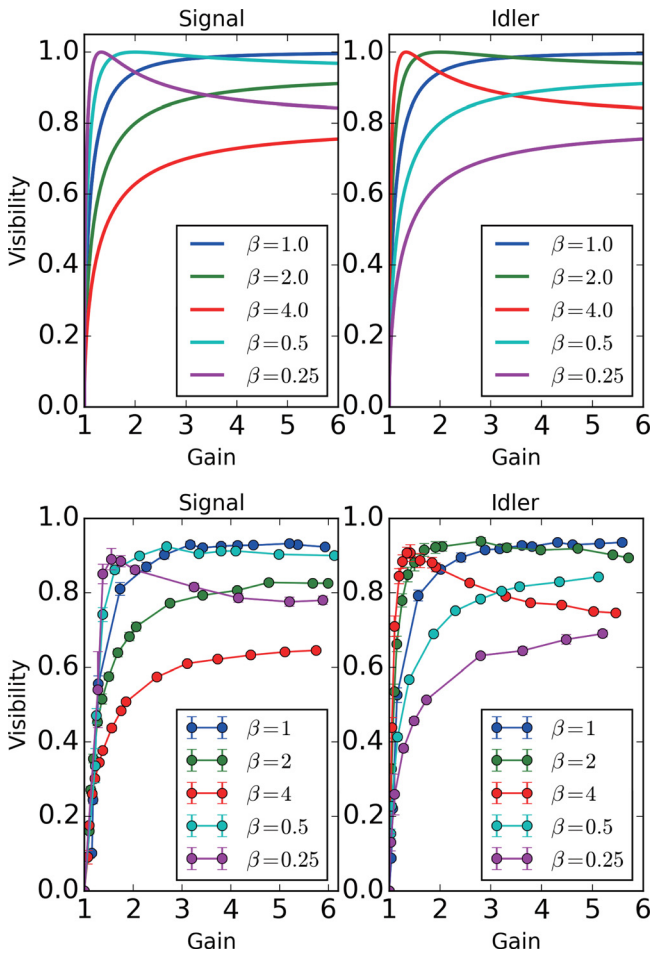

FIG. 4. The intensity ratio and intensity gain dependence of the two output port visibilities. Top left and right, the theoretical simulations from Eqs. (5) and (6), bottom, the experimental results for the signal and idler outputs.

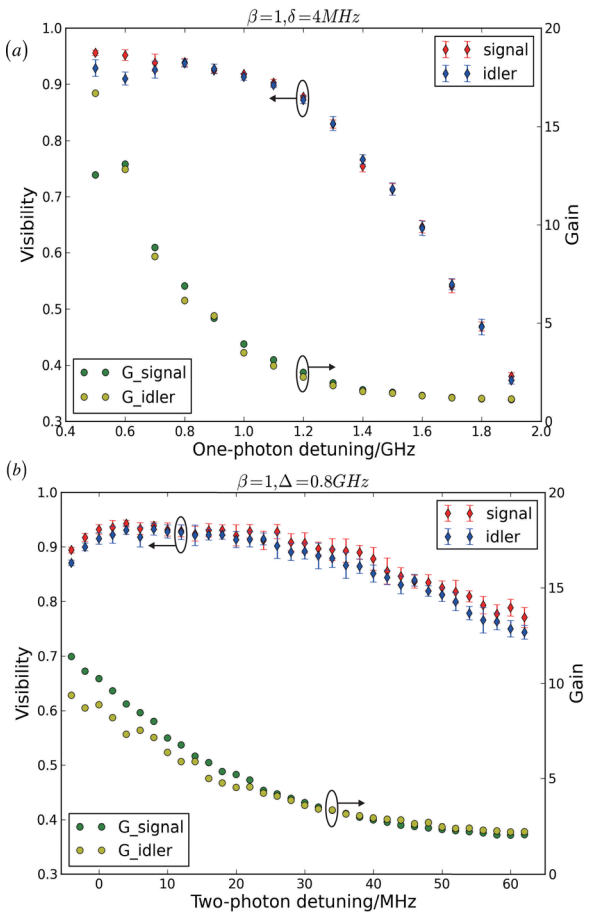

FIG. 5. (a) The visibilities of the signal and idler fringe as a function of one-photon detuning. (b) The visibilities of the signal and idler fringe as a function of two-photon detuning. The intensity gains for both beams are also depicted in both figures.

depend on the phase of the three beams. Under amplification condition, quantum correlation shared between the two output ports of the PSA stage will be enhanced. Under de-amplification condition, the second PA can recover the signal and idler beams back to the initial states (coherent state and vacuum). Instead of being seeded by two noisy signal and idler beams, the current system described in this letter is seeded by two coherent states. When the system operates at amplification condition, it will generate two output beams with intensity difference squeezing, and at de-amplification condition, these two outputs will show intensity sum squeezing as predicted by our theoretical study.[33] We believe it is worth studying how the sensitivity of the interferometer changes if we apply the system studied here to the first stage of the SU (1,1) interferometer.

In conclusion, we have experimentally built a nonlinear beamsplitter using a PA, which is based on non-degenerated FWM process in hot rubidium vapor and studied the interference phenomena. It should be noted that a non-degenerate parametric amplifier with two coherent seeding beams has also been studied in parametric down conversion in a nonlinear crystal putting in a cavity.[3,34,35] However, there are several distinctions between our scheme presented here and the previous works[3,34,35] based on nonlinear crystal due to the advantages of the FWM process in atomic vapor, such as no need of cavity, multimode nature, and natural separation of the output beams. We find that the intensity ratio of the two input beams can affect the visibilities of the two output ports. The better intensity balancing of the two input beams gives better visibilities of the two output ports at high gain regime. We also studied how the one- and two-photon detunings influence the visibilities. Our studies here pave the way to study the quantum properties of squeezing and entanglement predicted by our recent theoretical work.[33] Such a nonlinear beamsplitter could be used to construct a nonlinear interferometer which is different from our previous SU (1,1) interferometer. It may also find applications in phase-sensitive generation of entangled images.

This work was supported by the National Natural Science Foundation of China under Grant Nos. 91436211, 11374104 and 10974057, the SRFDP (20130076110011), the Program for Professor of Special Appointment (Eastern Scholar) at Shanghai Institutions of Higher Learning, the Program for New Century Excellent Talents in University (NCET-10-0383), the Shu Guang project supported by Shanghai Municipal Education Commission and Shanghai Education Development Foundation (11SG26), the Shanghai Pujiang Program under Grant No. 09PJ1404400, the Scientific Research Foundation of the Returned Overseas Chinese Scholars, State Education Ministry, and Program of State Key Laboratory of Advanced Optical Communication Systems and Networks (2016GZKF0JT003).

[1]H. A. Bachor and T. C. Ralph, *A Guide to Experiments in Quantum Optics* (Wiley-VCH Verlag GmbH & Co. KGaA, 2004).
[2]T. Aoki, N. Takei, H. Yonezawa, K. Wakui, T. Hiraoka, A. Furusawa, and P. van Loock, Phys. Rev. Lett. **91**, 80404 (2003).
[3]J. Jing, J. Zhang, Y. Yan, F. Zhao, C. Xie, and K. Peng, Phys. Rev. Lett. **90**, 167903 (2003).
[4]P. van Loock, C. Weedbrook, and M. Gu, Phys. Rev. A **76**, 32321 (2007).
[5]X. Su, S. Hao, X. Deng, L. Ma, M. Wang, X. Jia, C. Xie, and K. Peng, Nat. Commun. **4**, 2828 (2013).
[6]S. Yokoyama, R. Ukai, S. C. Armstrong, C. Sornphiphatphong, T. Kaji, S. Suzuki, J. Yoshikawa, H. Yonezawa, N. C. Menicucci, and A. Furusawa, Nat. Photonics. **7**, 982 (2013).
[7]C. Weedbrook, S. Pirandola, R. García-Patrón, N. J. Cerf, T. C. Ralph, J. H. Shapiro, and S. Lloyd, Rev. Mod. Phys. **84**, 621 (2012).
[8]M. Chen, N. C. Menicucci, and O. Pfister, Phys. Rev. Lett. **112**, 120505 (2014).
[9]J. Roslund, R. M. de Araujo, S. Jiang, C. Fabre, and N. Treps, Nat. Photonics **8**, 109 (2014).
[10]J. Jing, C. Liu, Z. Zhou, Z. Y. Ou, and W. Zhang, Appl. Phys. Lett. **99**, 011110 (2011).
[11]J. Kong, J. Jing, H. Wang, F. Hudelist, C. Liu, and W. Zhang, Appl. Phys. Lett. **102**, 011130 (2013).
[12]F. Hudelist, J. Kong, C. Liu, J. Jing, Z. Y. Ou, and W. Zhang, Nat. Commun. **5**, 3049 (2014).
[13]B. Yurke, S. L. McCall, and J. R. Klauder, Phys. Rev. A **33**, 4033 (1986).
[14]W. N. Plick, J. P. Dowling, and G. S. Agarwal, New J. Phys. **12**, 83014 (2010).
[15]C. F. McCormick, V. Boyer, E. Arimonda, and P. D. Lett, Opt. Lett. **32**, 178 (2007).
[16]C. F. McCormick, A. M. Marino, V. Boyer, and P. D. Lett, Phys. Rev. A **78**, 043816 (2008).
[17]C. Liu, J. Jing, Z. Zhou, R. C. Pooser, F. Hudelist, L. Zhou, and W. Zhang, Opt. Lett. **36**, 2979 (2011).
[18]Z. Qin, J. Jing, J. Zhou, C. Liu, R. C. Pooser, Z. Zhou, and W. Zhang, Opt. Lett. **37**, 3141 (2012).
[19]V. Boyer, A. M. Marino, R. C. Pooser, and P. D. Lett, Science **321**, 544 (2008).
[20]A. M. Marino, R. C. Pooser, V. Boyer, and P. D. Lett, Nature **457**, 859 (2009).
[21]R. C. Pooser, A. M. Marino, V. Boyer, K. M. Jones, and P. D. Lett, Phys. Rev. Lett. **103**, 010501 (2009).
[22]V. Boyer, C. F. McCormick, E. Arimondo, and P. D. Lett, Phys. Rev. Lett. **99**, 143601 (2007).
[23]R. T. Glasser, U. Vogl, and P. D. Lett, Phys. Rev. Lett. **108**, 173902 (2012).
[24]R. M. Camacho, P. K. Vudyasetu, and J. C. Howell, Nat. Photonics **3**, 103 (2009).
[25]A. MacRae, T. Brannan, R. Achal, and A. I. Lvovsky, Phys. Rev. Lett. **109**, 033601 (2012).
[26]U. Vogl, R. T. Glasser, J. B. Clark, Q. Glorieux, T. Li, N. V. Corzo, and P. D. Lett, New J. Phys. **16**, 013011 (2014).
[27]J. B. Clark, R. T. Glasser, Q. Glorieux, U. Vogl, T. Li, K. M. Jones, and P. D. Lett, Nat. Photonics **8**, 515 (2014).
[28]Z. Qin, L. Cao, H. Wang, A. M. Marino, W. Zhang, and J. Jing, Phys. Rev. Lett. **113**, 023602 (2014).
[29]R. C. Pooser and B. Lawrie, Optica **2**, 393 (2015).
[30]C. S. Embrey, M. T. Turnbull, P. G. Petrov, and V. Boyer, Phys. Rev. X **5**, 031004 (2015).
[31]Y. Cai, J. Feng, H. Wang, G. Ferrini, X. Xu, J. Jing, and N. Treps, Phys. Rev. A **91**, 13843 (2015).
[32]R. Pooser and J. Jing, Phys. Rev. A **90**, 43841 (2014).
[33]Y. Fang and J. Jing, New J. Phys. **17**, 23027 (2015).
[34]Y. Zhang, H. Wang, X. Li, J. Jing, C. Xie, and K. Peng, Phys. Rev. A **62**, 023813 (2000).
[35]X. Li, Q. Pan, J. Jing, J. Zhang, C. Xie, and K. Peng, Phys. Rev. Lett. **88**, 047904 (2002).